



1 **Direct observation of molecular clusters and nucleation**
2 **mode particles in the Amazon**

3
4 **Daniela Wimmer¹, Stephany Buenrostro Mazon¹, Hanna Elina Manninen^{1,2}, Juha**
5 **Kangasluoma¹, Alessandro Franchin^{1,3,4}, Tuomo Nieminen^{1,5}, John Backman⁶,**
6 **Jian Wang⁸, Chongai Kuang⁸, Radovan Krejci⁷, Joel Brito^{9,10}, Fernando**
7 **Goncalves Morais⁹, Scot Turnbull Martin¹¹, Paulo Artaxo⁹, Markku Kulmala¹,**
8 **Veli-Matti Kerminen¹ and Tuukka Petäjä¹**

9
10 ¹Department of Physics, University of Helsinki, Gustaf Hallströmin katu 2a, 00560, Helsinki,
11 Finland

12 ²European Organization for Nuclear Research (CERN), 1211 Geneva, Switzerland

13 ³NOAA Earth System Research Laboratory (ESRL), Chemical Sciences Division, Boulder,
14 CO, USA

15 ⁴Cooperative Institute for Research in Environmental Sciences, University of Colorado
16 Boulder, Boulder, CO, USA

17 ⁵Department of Applied Physics, University of Eastern Finland, Post Office Box 1627, 70211
18 Kuopio, Finland

19 ⁶Finnish Meteorological Institute, Atmospheric composition research, Erik Palménin aukio 1,
20 00560, Helsinki, Finland

21 ⁷Stockholm University, Department of Environmental Science and Analytical Chemistry
22 (ACES), 106 91 Stockholm, Sweden

23 ⁸Environmental and Climate Sciences Department, Brookhaven National Laboratory, Upton,
24 New York, USA

25 ⁹Institute of Physics, University of São Paulo, de Física, Universidade de São Paulo, Rua do
26 Matao 1371, CEP 05508-090, São Paulo, Brazil

27 ¹⁰Laboratory for Meteorological Physics (LaMP), Université Clermont Auvergne, F-63000
28 Clermont-Ferrand, France

29 ¹¹School of Engineering and Applied Sciences, Harvard University Cambridge, Massachusetts
30 02138, United States of America

31

32 *Correspondence to:* Daniela Wimmer (daniela.wimmer@helsinki.fi)

33 **Keywords:** atmospheric ions, particle formation, rainforest, high-frequency rainfall

34

35 **Abstract**

36 We investigated atmospheric new particle formation (NPF) in the Amazon rainforest using
37 direct measurement methods. The occurrence of NPF on ground level in the Amazon region
38 has not been observed previously in pristine conditions. Our measurements extended to two



39 field sites and two tropical seasons (wet and dry). We measured the variability of air ion
40 concentrations (0.8–20 nm) with an ion spectrometer between 2011 and 2014 at the T0t site
41 and between February and October 2014 at the GoAmazon 2014/5 T3 site. The main difference
42 between the two sites is their geographical location. Both sites are influenced by the Manaus
43 pollution plume yet with different frequencies. T0t is reached by the pollution about 1 day in
44 7, where the T3 site is about 15% of the time affected by Manaus. The sampling was performed
45 at ground level at both sites. At T0t the instrumentation was located inside the rainforest,
46 whereas the T3 site was an open pasture site. T0t site is mostly parallel wind to Manaus,
47 whereas T3 site is downwind of Manaus. No NPF events were observed inside the rainforest
48 canopy (site T0t) at ground level during the period Sep 2011- Jan 2014. However, rain-induced
49 ion and particle bursts (hereafter, “rain events”) occurred frequently (306/529 days) at T0t
50 throughout the year but most frequently between January and April (wet season). Rain events
51 increased nucleation mode (2-20 nm) particle and ion concentrations on the order of 10^4 cm^{-3} .
52 We observed 8 NPF events at the pasture site during the wet season. We calculated the growth
53 rates (GR) and formation rates of neutral particles and ions for the size ranges 2-3 nm, 3-7 nm
54 and 7-20 nm using the ion spectrometer data. One explanation for the absence of new particle
55 formation events at the T0t site could be a combination of cleaner airmasses and the rainforest
56 canopy acting as an ‘umbrella’, hindering the mixing of the airmasses down to the measurement
57 height. Neutral particle growth rates in the 3-7 nm regime showed two phenomena. Growth
58 rates were either about 2 nmh^{-1} or about 14 nmh^{-1} . There was no clear difference in the sulfuric
59 acid concentrations for NPF days vs days without NPF. Back trajectory calculations show
60 different air mass origin for the NPF days compared to non NPF days.

61

62 1 Introduction

63

64 Globally, atmospheric new particle formation (NPF) and growth has been estimated to account
65 for a major, if not dominant, fraction of atmospheric cloud condensation nuclei (Merikanto et
66 al. 2009, Wang and Penner, 2009, Yu and Luo, 2009, Dunne et al., 2016; Kulmala et al., 2016).
67 The formation of atmospheric nanoparticles is a multi-stage process, in which stable clusters
68 form from gas phase precursors followed by the activation of these clusters for further growth
69 (Kulmala et al. 2014). Although atmospheric NPF is occurring frequently in many
70 environments (e.g. Kulmala et al. 2004, Manninen et al. 2010), the Amazon basin is one of the
71 locations where the initial steps of the formation of nanoparticles have not been previously
72 observed from ground based measurements (Martin et al, 2010). In the Amazon, emissions and



73 oxidation of volatile organic compounds (e.g. Lelieveld et al. 2008), aerosol activation to cloud
74 droplets, and eventually rain formation, are tightly connected and interlinked with
75 meteorological processes, such as the boundary layer development and deep convection (Wang
76 et al., 2016). Aerosol concentrations in the atmosphere are rapidly changing with deforestation
77 and the associated biomass burning and economic development in the Amazon region (Martin
78 et al. 2016, Artaxo et al., 2013).

79 The Manaus metropolis (population 2 million) is the capital of the state of Amazonia, Brazil,
80 surrounded by the largest rainforest on Earth, as shown in Fig 1 (Martin et al, 2017). The
81 measurements discussed in this paper took place at two different locations in the Amazon
82 rainforest: a clearing site 70 km downwind from Manaus (T3; Martin et al., 2016), and a site
83 inside the rainforest canopy, mostly unaffected by Manaus pollution (T0t; Martin et al., 2010b).
84 The sites will be described in more detail in section 2.1. Depending on the wind direction, these
85 sites can represent (i) one of the most natural continental locations on Earth, or (ii) a location
86 affected by both polluted metropolis and rainforest (Martin et al., 2016). The regular synoptic
87 changes between the wet and dry seasons offered an additional important scientific contrast to
88 study aerosol dynamics. During most of the wet season the Amazon basin is one of the cleanest
89 continental regions on Earth (Andreae, 2007; Martin et al., 2010a, Artaxo et al., 2013, Andreae
90 et al., 2015), while during the dry season biomass burning and local fire emissions are
91 ubiquitous throughout the basin. Additionally, our study region experiences frequent high-
92 intensity precipitation episodes.

93 The primary goal of this paper was to investigate the occurrence of new particle formation
94 (NPF) and growth in the Amazon region, and to quantify the role of ions and aerosol particles
95 in this process. No NPF events were observed during the long-term measurements at the site
96 largely unaffected by Manaus emissions. A clear correlation between rain intensities and ion
97 concentrations was found for both measurement sites. At the more polluted pasture site, we
98 observed 8 NPF events, which occurred during the wet season. The data from comprehensive
99 measurements shows that the freshly formed particles were growing to sizes of about 60 nm at
100 which they start to act as cloud condensation nuclei.

101 **2 Methods**

102 The measurements discussed here were conducted in 2014 outside the rainforest canopy as a
103 part of the Green Ocean Amazon (GoAmazon2014/5) Experiment (Martin et al., 2016), which



104 was going on for the period from 1 January 2014 to 31 December 2015. GoAmazon2014/5 was
105 designed to study the perturbation in cloud and aerosol dynamics by the Manaus emissions.
106 Our measurement campaign took place during 28 January – 13 October 2014 near the city of
107 Manacapuru, Brazil, 70 km downwind of Manaus. We compare the campaign data to long-
108 term measurements made between September 2011 and January 2014.

109

110 **2.1. Measurement sites**

111 **2.1.1 Inside canopy measurements**

112 The T0t ecological reserve (Martin et al, 2010b) is a terrestrial ecosystem science measurement
113 site located 60 km north of the Manaus metropolis in the central region of Brazil (-2.609°S, -
114 60.2092°W). Manaus is situated at the confluence of the Black River (Rio Negro) with the
115 Solimões river, which together form the Amazon river. The city is an isolated urban region
116 with a population of more than 2 million people (IBGE, 2015; Martin et al., 2017) and is
117 surrounded by 1500 km of forests in all directions. T0t is mostly unaffected by the Manaus
118 pollution and is surrounded by dense rainforest. It allows the characterization of an almost
119 completely undisturbed natural environment (Martin et al, 2016). The rainforest canopy is
120 homogeneous with an average height of 30 m. A Neutral cluster and Air Ion Spectrometer
121 (NAIS) was placed inside a hut within the rainforest canopy, with an inlet system 2 m above
122 the ground level. In addition to the ion spectrometer measurements, the measurement hut hosts
123 a Vaisala system (WXT520) for acquiring meteorological parameters and a differential
124 mobility particle sizer (DMPS). The DMPS was sampling from an inlet 60 m above the ground
125 level, therefore sampling aerosols above the canopy. Both the DMPS and the NAIS were
126 measuring at the T0t site from 2011-2014. For the GoAmazon2014/5 campaign it was moved
127 to a measurement site outside the rainforest canopy, which is described in Section 2.1.2. The
128 nucleation and growth rates reported here were all determined from the direct measurements
129 provided by the NAIS.

130 **2.1.2 Outside canopy measurements**

131 T3 is a site equipped with an Atmospheric Radiation Measurement (ARM) Climate Research
132 Facility of the United States Department of Energy, 70 km downwind of the city of Manaus (-
133 3.2133°S, -60.5987°W; Mather et al., 2014) and included an ARM Mobile Aerosol Observing
134 System (MAOS). The site is located in a pristine environment where the Manaus pollution



135 plume regularly intersects. Under the day-to-day variability in the meteorology, both clean and
136 polluted air masses, mixed to variable degrees, arrived at T3. The site is located in a clearing
137 of the rainforest where the canopy did not hinder mixing. This site also hosted numerous
138 instrument systems from other GoAmazon2014/5 participants (Martin et al., 2016). The same
139 NAIS used at T0t was deployed at T3 from end of January 2014 onwards. Sub-3 nm neutral
140 particle measurements were done with a Particle Size Magnifier (PSM). The PSM and NAIS
141 inlets sampled at 2 meters from ground level in an open clearing.

142

143 2.2 Instrumentation

144 2.2.1 Neutral cluster and Air Ion Spectrometer (NAIS)

145 A Neutral cluster and Air Ion Spectrometer (NAIS; Manninen et al., 2016) was used to
146 determine the early stages of atmospheric nucleation and subsequent growth. The NAIS
147 measures the mobility distributions in the range $3.2\text{--}0.0013\text{ cm}^2\text{V}^{-1}\text{ s}^{-1}$, which corresponds to
148 a mobility diameter range of 0.8–42 nm. The ion and particle size distributions are measured
149 in three different stages: ion, particle and offset. The NAIS consists of two parallel cylindrical
150 DMA's (Differential Mobility Analyzers), one for classifying negative ions and the other for
151 positive ions. When in ion mode, corona chargers and electrostatic filters are switched off to
152 allow only naturally charged ions into the DMA. During the neutral particle mode, the particles
153 are charged and then filtered by an electrostatic filter to neutralize them before entering the
154 DMA. The inlet flow into the NAIS is 60 liters per minute (LPM), whereas the sample and the
155 sheath flows of the DMA's are 30 and 60 LPM, respectively. The NAIS time resolution was
156 set to 5 min, where a measurement cycle of negative ions, positive ions, and total particles is
157 included.

158 The instrument and calibration are described in more details in Asmi et al. (2009), Wagner et
159 al. (2016) and Manninen et al. (2016). The accuracy of the ion concentration of the NAIS was
160 estimated to be 10-30%, which was mainly due to flow rate uncertainties (Manninen et al.,
161 2016; Wagner et al., 2016). During the campaign, the deposition of particulate matter inside
162 the instrument caused decreasing flow rates between the maintenance periods. This may have
163 further increased the uncertainty in measured particle sizes and number especially at sizes
164 bigger than 20 nm.

165



166

167 **2.2.2 Particle Size Magnifier (PSM)**

168 The instrument we used to determine aerosol particle concentrations at sizes below 3 nm was
169 a Particle Size Magnifier (PSM; Airmodus A09; Vanhanen et al., 2011). The PSM is a mixing-
170 type condensation particle counter (CPC), in which the aerosol is turbulently mixed with air
171 saturated with diethylene glycol (DEG). DEG only grows the particles to about 90 nm, so the
172 PSM system consists of a second stage, where the particles are grown to optically detectable
173 sizes. The 50% activation diameter of the instrument can be varied in size range 1–4 nm in
174 mobility diameter (Vanhanen et al., 2011) by changing the mixing ratio of the saturator and
175 sample flows. At GoAmazon2014/5, the PSM was used in scanning mode. In scanning mode,
176 the saturator flow is continuously changing, altering the cut-off diameters from 1-4 nm. One
177 scan takes 4 min and the system was setup to do one upscan, followed by a downscan. Due to
178 the challenging measurement conditions, the size resolved data could not be used for the
179 analysis.

180 Prior to the deployment during the GoAmazon2014/5 campaign, the PSM was equipped with
181 an inlet system, especially designed to decrease the relative humidity of the sample without
182 disturbing the sample itself and maintaining high flow rates (10 Lpm) until the actual sampling
183 to minimize diffusion losses. Laboratory studies have shown that the RH affects the counting
184 efficiency of the PSM drastically (higher sensitivity at smaller sizes at higher RH). The PSM
185 with the inlet was calibrated, using limonene and its oxidation products (Kangasluoma et al,
186 2014) as the test aerosol. We expect the aerosol sample in Brazil to be mostly organic species,
187 hence the decision to calibrate with limonene. The resulting lowest cut-off diameter of the PSM
188 was 1.5 nm (± 0.3 nm). The estimated error is a combination of calibration uncertainty and the
189 influence of the ambient RH on the cut-off diameter of the PSM. To our knowledge, this is the
190 first time when results from ground-based sub-3 nm aerosol particle measurements are shown
191 for the Amazon rainforest. In total, 38 days of data obtained during the dry season were used.

192 **2.2.3 Supporting instrumentation at T0t site**

193 Submicron aerosol number size distributions and total particle number concentrations were
194 monitored with a DMPS system (Aalto et al., 2001) and a CPC. The time resolution of the CPC
195 with a cut-off of about 6 nm was 1 minute. The DMPS measured number size distributions
196 over the mobility diameter range of 6–800 nm (Backman et al., 2012). The complete size



197 distribution is obtained in a 10-minute time resolution. The DMPS system was designed so that
198 the size segregated aerosols were measured for 8 minutes and for the remaining 2 minutes of
199 the 10 min cycle, total particle number concentrations were measured with the CPC directly
200 using a bypass valve. The line losses for the DMPS were estimated to be about 50% for particles
201 smaller than 4 nm in diameter for a similar setup during the AMAZE-08 Experiment (Martin
202 et al., 2010). For the measurements reported here, a similar setup with a 60 m sampling line
203 was used. The DMPS data reported here is qualitative but not quantitative. Formation and
204 growth rates were analyzed using NAIS data only. Meteorological data from a Vaisala weather
205 station included temperature, relative humidity, wind speed and wind direction, and
206 precipitation intensity.

207 **2.3 Measurement periods: wet and dry season**

208 The changes between tropical seasons - the wet and dry seasons - offered an additional
209 comparison between two contrasting environmental conditions (Martin et al., 2016, Artaxo et
210 al., 2013). The particle population is in dynamic balance with the ecosystem and anthropogenic
211 contributions (e.g. biomass burning; which produces them directly and indirectly) and the
212 hydrological cycle (which removes them). In the wet season (December to March), the Manaus
213 plume aside, the Amazon basin is one of the cleanest continental regions on Earth (Andreae,
214 2007; Martin et al., 2010). In the dry and transition season (April to September), biomass
215 burning emissions are prevalent throughout the basin. The most intense biomass burning and
216 atmospheric perturbations take place at the southern and eastern edges of the forest (Brito et
217 al., 2014), however their transport impact the whole basin. Wet deposition decreases whereas
218 condensation sink increases during the dry season. That leads to an overall increase in aerosol
219 concentration in the accumulation mode of about one order of magnitude even in remote areas
220 (Artaxo et al., 2013). Planetary boundary layer development has also a seasonal behavior:
221 stable nocturnal layer and a strong vertical mixing during daytime. The vertical mixing can be
222 enhanced during the wet season due to convective clouds. The nocturnal layer on the other
223 hand traps the emissions near the surface, which can be more pronounced during dry season,
224 as biomass burning usually starts at midday and continues into evening hours (Martin et al,
225 2010).

226 **2.4 Data analysis**



227 All the available data from the NAIS was cleaned for potential instrumental noise. The cleaning
228 process was done visually using the particle and ion size distributions as surface plots. The
229 NAIS can measure both naturally charged ions and neutral particle size distributions. We
230 present data from both measurements in the following. Based on this initial screening, the
231 decision was made whether one or more of the electrometers was reliable or not and the non-
232 reliable data was removed. On 44.7% of the days the cleaning procedure was applied. Mostly
233 the particle data in the smaller size ranges (up to 3 nm) was unreliable. The procedure follows
234 the guidelines introduced by Manninen et al., 2010. We observed an unexplained increase in
235 the concentrations of the cluster ions in the NAIS towards the end of October 2013 to January
236 2014 at the T0t site. This increased level continued when the NAIS was taken to the T3 site.
237 By comparing the 2014 concentrations of the NAIS channels to those prior to the increase
238 (January 2012 and 2013), a correction factor of 1.8 was applied to the first 4 NAIS channels
239 (0.8-1.25 nm) to account for the drift for the subsequent data.

240 Rain-induced ion events were selected as a day which included an ion burst coincided with the
241 onset of precipitation. Median and maximum (95 percentile) ion concentrations were calculated
242 during the time when the rain intensity was $>0 \text{ mm hr}^{-1}$ ($>0.1 \text{ mm hr}^{-1}$ for the T3 site, as the
243 rain data from the T3 site showed some rain signal on almost all of the days). In some of the
244 days, rain occurred sporadically several times per day. In order to take this into account, two
245 separate rain events were classified as such if they occurred $>1 \text{ hr.}$ apart from the end of the
246 first and the start of the second. Any fluctuations in the rain intensity for a shorter time period
247 than 1 hr. was considered to be part of a single rain event.

248 The new particle formation event analysis from the ion spectrometer data, including the event
249 classification and formation and growth rate calculations, followed the already well-defined
250 guidelines (Kulmala et al., 2012). In the data analysis, the first step was to classify all available
251 days into NPF event and non-event days according to methods introduced earlier by Hirsikko
252 et al. (2007) and Manninen et al. (2010). The days which do not fulfill the criteria of an event
253 or non-event day, are categorized as undefined days. However, no days were classified as
254 undefined days in this study. The classification was done visually using daily contour plots of
255 particle number size distributions. The second step in the analysis was to calculate various
256 quantities related to each NPF event, such as the particle growth rate (GR) and formation rate
257 (J). Both growth and formation rates were calculated for three different size bins (2-3 nm, 3-7
258 nm and 7- 20 nm in diameter) using both ion and neutral particle data from the NAIS. The



259 particle growth rate was determined by finding the times at which the maximum concentrations
260 of ions/particles in each of these size bins occurred. A fit between the points was then applied
261 to determine the GR. The particle formation rate was determined for lower end of each size bin
262 (2, 3 and 7 nm) by taking into account the growth rates, condensation sink and coagulation
263 sink.

264 **3 Results**

265 All the times mentioned below are local Manaus time (LT), which is Coordinated Universal
266 Time (UTC) –4 h.

267 **3.1 Number concentrations of ions and particles at the two sites**

268 An overview of the observed number concentrations of ions and particles as well as ambient
269 conditions at the two measurement sites is presented in Table 1. We divided the measured ions
270 into three sub-size ranges: cluster ions (0.8-2 nm), intermediate ions (2-4 nm) and large ions
271 (4-20 nm) and the same for neutral particles. The lower and upper limits of the intermediate
272 ion size range vary in the scientific literature (see Hirsikko et al., 2011 and references therein).
273 Here, 2-4 nm was chosen, as this size range seems to work well in differentiating between
274 atmospheric new particle events and non-events when using ion measurements (Leino et al.,
275 2016). Additionally, the wet and dry seasonality characteristic for the Amazon (Martin et al.
276 2010) can be observed in the concentration of the large ions (4-20nm): the biomass burning
277 during the dry season is expected to increase large ion concentrations, whereas during the wet
278 season their concentrations are expected to decrease due to wet deposition and reduced source
279 strengths.

280 Particle and ion concentrations were, in general, higher at the open pasture T3 site, downwind
281 of Manaus. The average concentrations of 4 – 20 nm particles were a factor of 3 higher in
282 comparison to parallelwind of Manaus and inside the canopy (T0t). The environmental
283 variables were relatively similar between the two sites, the temperature and RH being slightly
284 lower at the outside canopy site compared with the inside canopy site.

285

286 **3.1.1 Inside rainforest canopy site (T0t)**



287 Figure 2 shows the seasonal variability of ions and particles in the three size ranges (0.8-2nm,
288 2-4 nm and 4-20 nm) for the 2011-2014 period. The cluster ions had a median concentration
289 of 723 cm^{-3} and 879 cm^{-3} for negative and positive ions, respectively. These medians are higher
290 than those found in several other locations (eg. urban Paris, Dos Santos et al. 2015; coastal
291 Mace Head, Vana et al. 2008 and Finokalia, Kalvitis et al. 2012; Puy de Dome, Rose et al.
292 2016), but comparable to those reported at a boreal forest site in Hyytiälä, Finland (Hirsikko et
293 al. 2005). Higher cluster ion concentrations have been reported in an Australian rainforest in
294 Tumbarumba (Suni et al. 2008) and in a wetland site in Abisko (Svennigsson et al., 2008), both
295 sites having concentrations of ~ 2400 (1700) cm^{-3} for negative (positive) ions. The size bin of
296 2-4 nm had a median concentration of $5\text{--}10 \text{ cm}^{-3}$ for both negative and positive ions. Large
297 ions 4–20 nm had a median negative (positive) ion concentration of 85 (153) cm^{-3} when
298 considering the 149 days (out of 524 days), that had data for this size range. These values are
299 comparable, for example, to intermediate and large ion concentrations found in coastal Mace
300 Head (Vanta et al. 2008) outside the periods of rain or active NPF. Cluster ion concentrations
301 are clearly higher in Oct-Dec for both seasons. In general, the positive cluster ion
302 concentrations are higher in all the cluster ion and intermediate ion size classes for all the
303 months. Table 2 summarizes the annual concentrations of ions and total particles for the three
304 size bins.

305 Differences between the wet (Dec-Mar) and dry and transition season (Apr-Oct) were also
306 observed in the diel cycle of the ion and particle concentration. Positive and negative cluster
307 ion concentrations were, on average, higher during the wet season compared to the dry season.
308 In both seasons, there were more positive than negative cluster ions (Table 1). The lower
309 concentrations of negative ions are expected due to the Earth's ground 'electrode' effect, in
310 which negative ions are pushed away from the Earth surface (Hoppel W. A., 1967).
311 Additionally, cluster ions (0.8-2 nm) showed slightly higher concentrations in the morning and
312 evening, compared to other times of the day. Enhanced median cluster ion concentrations in
313 the early morning have also been reported elsewhere, likely due to higher radon concentration
314 levels at that time of the day (Hirsikko et al 2011 and references therein). A dip in the median
315 ion concentration after midday coincides with a higher median concentration of large ions,
316 which is a sign of a larger sink for cluster ions. Intermediate and large ions (2-4nm and 4-20
317 nm) had only one daytime peak in their concentration in both seasons, similar to the total
318 particle concentrations shown in Figure 3. For 2–4 nm ions, this occurred in the late afternoon
319 and was more pronounced during the wet season compared with the dry season for both



320 polarities. The peak does not seem to be a result of the wet season's rain-induced ion bursts
321 (Horrak et al. 1998), as discussed in more detail in Section 3.2. Lastly, 4-20 nm ions peaked at
322 around midday during the wet season, while their diel pattern was more irregular during the
323 dry season. The negative 4-20 nm ions had the highest concentrations ($>1000\text{ cm}^{-3}$) during the
324 dry season, most likely due to biomass burning and weaker wet deposition. This feature could
325 not be observed for positive large ions.

326 The total concentrations of 2-4 nm and 4-20 nm neutral particles had similar daytime peaks
327 with otherwise stable night-time concentrations (Fig. 3). The median concentration of 2-4 nm
328 neutral particles was $\sim 500\text{ cm}^{-3}$, which about a factor 100 higher than the median concentration
329 of 2-4 nm ions. Similar to ions in the same size range, 4-20 nm particles peaked at around
330 midday, reaching values of about 1000 to 2000 cm^{-3} .

331 3.1.2. Outside rainforest canopy site (T3)

332 The median ion and particle number concentrations during the wet and dry season at the T3
333 site, outside the canopy and downwind of Manaus, are given in Table 1. The diel cycles of ion
334 and neutral particle concentrations at this site appeared to be very similar in both wet and dry
335 season. The cluster ions showed a clear 24 hr cycle: in the mornings (00:00-07:00) their
336 concentrations were $\sim 1500\text{ cm}^{-3}$ for negative ions, then decreased to $\sim 1000\text{ cm}^{-3}$ and eventual
337 increased back to $\sim 1500\text{ cm}^{-3}$ after 18:00. This daytime decrease in the concentration is most
338 likely due to the dilution of the boundary layer. The intermediate ions (2-4 nm) showed higher
339 concentrations between 03:00 and 06:00 during the dry season compared with the wet season.
340

341 The total particle concentration measured by the MAOS CPC ($>10\text{ nm}$ total particle
342 concentration) did not show any diel seasonal cycle. The median total particle concentrations
343 were about a factor of two higher during dry season (about 1500 cm^{-3}) compared with the wet
344 season (about 700 cm^{-3}).
345

346 3.2 Rain-induced ion formation events at inside canopy measurement site

347 While no NPF events were observed inside canopy (site T0t), rain-induced ion burst events
348 (hereafter, rain-events) were common and observed during 306 out the 524 measurement days.
349 Since multiple rain episodes could occur in a single day, each rain event was investigated
350 separately, giving a total of 579 rain-events. Figure 4 shows an example of multiple rain-events



351 that took place during 24 January 2013 (wet season). It is clear from this figure that the negative
352 ions in the size ranges of 1-3 nm and 3-7 nm increased during the precipitation. A similar
353 feature for 2-8 nm negative ions during rain events has also been reported for an Australian
354 rainforest (Suní et al. 2008). Positive ions increased only in the 3-7 nm size range, and showed
355 even a decrease in the 1-3 nm size range during the time of the precipitation.

356

357 Rain-induced bursts are likely a result of a balloelectric effect, in which splashing water
358 produces intermediate ions such that the negative ions are smaller than the positive ions
359 (Horrak et al., 2005, Hirsikko et al., 2007, Tammet et al., 2009). The duration of the 579 rain
360 events varied from a couple of minutes to 22 hours, with over half the rain events lasting for
361 two hours or less. The rain events were more common during the wet season (Fig. 5) when also
362 the median rain intensity was higher. Although less frequent, rain-induced particle bursts were
363 also observed during the dry season. Wang et al., 2016 reported the production of small aerosol
364 particles, as a result of new particle formation at cloud outflow regions and further transport
365 into the boundary via strong convection during precipitation events in the Amazon. In the study
366 by Wang et al. the <20 nm particle concentrations decrease very rapidly, therefore we suggest
367 the process that we observe to be a local one, as described above. Also the production of ions
368 we observed only lasted for the duration of the precipitation, whereas Wang et al., observed a
369 change in the size spectrum that lasted for hours even after the precipitation event.

370 Figure 6 shows the relation between the median ion concentration and rain intensity during
371 each rain event. While no clear correlation between these two quantities was found, some
372 specific features were apparent. First, at the inside canopy site (T0t), the highest cluster ion and
373 2-4 ion concentrations occurred almost entirely during rather strong rain intensities. Second, at
374 the site outside the rainforest canopy (T3) shown in the same Figure for comparison, some log-
375 linear relation between the ion concentration and rain intensity could be observed for rain
376 intensities >1 mm h⁻¹ for all the three size bins.

377 Rain events were evident also when looking at the total particle concentrations measured by
378 the NAIS, as depicted in Figure 7. In this example, the rain intensity seemed to have two peaks,
379 one at ~09:00 followed by a second one at ~11:00. The ion and particle concentrations followed
380 these two peaks closely. Additionally, the DMPS data showed an appearance of nucleation
381 mode particles between 6 and 10 nm following the onset of rain. The DMPS was sampling at
382 a height of 60 m, which is well above the rainforest canopy. The concentration of these 6-10



383 nm particles increased to $\sim 20 \text{ cm}^{-3}$ during the rain event, while being below 5 cm^{-3} throughout
384 the day outside this peak. The 10-20 nm particle concentration showed first a decrease followed
385 by a slight increase up to $\sim 35 \text{ cm}^{-3}$, peaking later than the 6-10 nm particles. However, it is
386 unlikely that these are the same rain-induced burst as seen inside the canopy, as the total particle
387 concentrations seen by the NAIS were of the order of 10^4 cm^{-3} in the size bin of 4-20 nm. Wang
388 et al. (2016) reported that nucleation mode particles produced in cloud outflows will be
389 transported down with the rain, such that they can be observed at the ground level as an increase
390 in nucleation and Aitken mode concentrations ($D_p < 50 \text{ nm}$). The appearance of 6-10 nm
391 particles with its peak concentration, and subsequent increase in the 6-20 nm particle
392 concentration, could present a similar scenario of small particles brought down from the free
393 troposphere. However, any possible above-canopy source would be masked by such high rain-
394 induced concentrations inside the canopy, and it is likely that the dense rainforest canopy would
395 filter small particles before reaching the ground.

396

397 **3.3 New particle formation events at T3**

398 Table 3 summarizes the overall statistics collected at the outside canopy site (T3). We observed
399 no NPF events during the dry season, while on 12% of the days during the wet season we could
400 observe NPF. Similar event frequency has been observed in Finnish boreal forest environment
401 during autumn for example (Kontkanen et al., 2017). An earlier study by Backman et al. (2012)
402 showed that in metropolitan area of São Paulo (population 20 million), Brazil, NPF events
403 occurred on 18% of the days.

404 From the NAIS measurements, a total of 113 days were available for the outside canopy
405 measurements. For the wet season, the data from 28 January until 31 March were used (64
406 days) and for the dry season the data from 29 August until 13 October was used (46 days). Due
407 to technical issues, no NAIS data were available for the period 1 April – 28 August 2014. The
408 PSM measurements were carried out during the dry season only. In total, 38 days of the PSM
409 data were used and the results are shown in Figure 8. The PSM was used in the scanning mode
410 but, due to challenging environmental conditions, only the data measured at the highest
411 supersaturation (total particle concentration at $> 1.5 \text{ nm}$) is shown.

412 The PSM shows a similar diel pattern as the cluster ion concentrations measured by the NAIS
413 (see Fig. 9). We observed a higher median concentration during the early morning (03:00-
414 06:00), a dip in this concentrations during the early afternoon (12:00-15:00), and then a higher



415 median concentration in the evening (18:00-24:00). This could be explained by the Carnegie
416 curve (Harrison, R. G. and Carslaw, K. S., 2003), which shows the diel variation of the
417 ionospheric potential.

418 We selected all eight NPF event days to characterize the behavior of ions and aerosol particles
419 during the particle formation bursts. A comparison of the diel cycle for particles and ions for
420 nucleation versus no nucleation event days is shown in Figure 9. The cluster ions showed a
421 clear diel cycle with higher concentrations in the morning and evening both for NPF and non
422 NPF days. A clear increase in the concentration of the intermediate ions (2-4 nm) occurred
423 during the NPF event days, which is due to the growth of the ions out of the cluster ion size
424 range (0.8-2 nm). The intermediate ion concentration increased at around 09:00 LT, suggesting
425 an onset of the particle formation after sunrise when the boundary layer rises and mixing starts.
426 The number concentration of 4-20 nm total particles rose within the time window (09:00-12:00
427 LT) during the nucleation events, while on non NPF days these particles showed highest
428 concentrations after the sunrise (06:00) and sunset (18:00). The total particle concentration
429 measured by the MAOS CPC showed a clear concentration increase on NPF event days starting
430 from 09:00, which clearly indicates that the particles had grown from the smaller sizes to >10
431 nm, which is the lowest detection limit of the MAOS CPC. No clear diel pattern from the
432 MAOS CPC measurements was visible on the non NPF days.

433 The type of NPF events that we observed are likely of regional nature, requiring relatively
434 homogenous air masses for at least a few hours (Vana et al., 2004, Manninen et al., 2010). The
435 most likely explanation that no new particle formation events have been observed at the T0t
436 site compared to the T3 site are either the lack of sources to form sulfuric acid in the more
437 remote site. Another explanation might be that the sampling at the less polluted T0t site was
438 performed within the canopy, so the mixing of the boundary layer is hindered by the presence
439 of the rainforest canopy. The gaps, or fluctuations, in the distinct shape of NPF could be caused
440 by some degree of heterogeneity in the measured air masses. All the NPF events occurred
441 during daytime, starting at around 09:00. Sunrise takes place at 06:00 in the Amazon basin. All
442 the NPF events occurred during the wet season, which might be due to the lower condensation
443 sink at this time of the year, as shown in Table 1. The median sulfuric acid concentrations as
444 measured by a quadrupole HOx CIMS (Martin et al, 2016, supplementary material) resulted in
445 about $9 \cdot 10^5 \text{ cm}^{-3}$ both for nucleation event days and no NPF days. Similar values have been



446 reported for Finnish boreal forest measurement site in autumn, where also about 12% of the
447 days were classified as nucleation event days (Kontkanen et al., 2017).

448 Back trajectory calculations using HYSPLIT ([http://ready.arl.noaa.gov/hypub-](http://ready.arl.noaa.gov/hypub-bin/trajtype.pl?runtype=archive)
449 [bin/trajtype.pl?runtype=archive](http://ready.arl.noaa.gov/hypub-bin/trajtype.pl?runtype=archive)) showed a clear difference in air mass origin arriving to the
450 measurement site between NPF and no NPF days. Back trajectories were calculated 24h
451 backwards, arriving at 13:00 UTC (09:00 LT) on the NPF days at 500m a. s. l. The same
452 calculations were performed for each day before/after an NPF day. If an NPF event occurred
453 on two consecutive days, the day after both events was used for the no NPF day back trajectory
454 calculations. On NPF days, the 50th percentile of air masses originate from about -1.6°S, -
455 56.5°E and 738.9 m a. s. l. On non NPF days, the back trajectory calculations show origin at -
456 2.6°S, -56.6°E and 537.4 m a. s. l. These air masses all originate from upstream of the Amazon
457 river, where the NPF day air mass originate from further north, which is dense rainforest.
458 Nevertheless, all air masses pass over Manaus before reaching the measurement site.

459 Fig. 10 shows an example of a NPF event observed at the outside canopy (T3) site for both
460 negative ion and total particle concentration, as measured by the NAIS. The median diameter
461 of the smallest particle mode measured by the MAOS SMPS decreased at the start of the NPF
462 event, followed by its continuous growth up to about 60 nm. The intermediate ion
463 concentrations showed a clear increase during this NPF event, starting at 09:00. Large particles
464 and ions (4-20 nm) also showed higher concentrations during the event, but with a time delay
465 of about 30 minutes, indicating the growth of the small clusters to bigger sizes.

466 Table 4 shows a comparison of the median particle and ion concentrations (25th – 75th
467 percentiles in brackets), as well as the condensation sink for the time window 09:00-12:00
468 between the NPF event and non-event days. Clearly, the condensation sink was lower for the
469 NPF event days (0.001 s⁻¹) compared with the non-event days (0.005 s⁻¹). We also compared
470 environmental variables, including the temperature, relative humidity, wind direction and
471 precipitation. The biggest differences were the factor of 1.6 higher median concentration of
472 intermediate (2-4 nm) ions for the event days. The environmental variables indicated that there
473 was no precipitation on any of the classified NPF days, while the median RH was 3% lower
474 and the median wind direction was 81.6° during event days compared to 105.6° during non-
475 event days. The temperature was relatively similar between the NPF event and non-event days.



476 Table 5 shows the calculated GR, particle formation rates and condensation sinks for each of
477 the classified NPF event day. Both these quantities were determined for three different size
478 ranges (2-3, 3-7 and 7- 20 nm), and calculated separately for the ion and particle data. The
479 results show considerably lower ion formation rates compared with neutral particle formation
480 rates, consistent with observations made at most other continental sites (Manninen et al., 2010;
481 Hirsikko et al., 2011). The growth rates of particles and ions were comparable to each other
482 and typically smaller for the 2-3 nm size range compared with the 3-7 and 7-20 nm size ranges.
483 An increase in the particle/ion growth rate with an increasing particle size has been reported
484 earlier in a few other sites (see Häkkinen et al., 2013, and references therein).

485 We observed two regimes when looking at the neutral 3-7 nm GR. On 3 days, the GR were
486 about 2 nm h^{-1} . Those days showed sulfuric acid concentrations of about $2 \cdot 10^6 \text{ cm}^{-3}$. According
487 to theoretical calculations about 10^7 cm^{-3} of sulfuric acid can account for 1 nm h^{-1} (Nieminen
488 et al., 2010). It is most likely that other compounds are participating to the growth. The other
489 NPF event days, showed GR of about 14 nmh^{-1} for the same 3-7 nm size range. On those days,
490 the sulfuric acid concentration was even lower (about $6 \cdot 10^5 \text{ cm}^{-3}$). These GR are most likely
491 driven by organic compounds (Tröstl et al., 2016). Tröstl et al. calculated that about 10^6 - 10^7 of
492 highly oxidized organic compounds are required to explain GR of about 10 nmh^{-1} .

493 **4 Summary and conclusions**

494 We performed direct observations of atmospheric new particle formation (NPF) events in the
495 Amazon area with state-of-the-art aerosol instrumentation. The measurement campaigns were
496 carried out at two observation sites (T0t and T3) in the vicinity of Manaus city in Brazil. One
497 of these sites was located inside the rainforest canopy (T0t), providing long-term (Sep 2011-
498 Jan 2014) measurement data to complement data from outside canopy site (T3).

499 No NPF events were observed inside the canopy during the period Sep 2011-Jan 2014.
500 However, we observed rain-induced ion and particle burst events (“rain-events”) inside the
501 canopy during 306 of the 529 days. Concentrations of 2-4 nm and 4-20 nm ions and total
502 particles were enhanced by up to 3 orders of magnitude during such rain-events ($\sim 10^4 \text{ cm}^{-3}$).
503 The rain events occurred throughout the year, but were most frequent during the wet season
504 (January to April) when also the median rain intensity was the strongest. Multiple rain events
505 could occur during the same day, totaling 579 rain events in 306 rainy days. The duration of
506 the rain events ranged from a couple of minutes to 22 hours, but over 50% of the events lasted



507 for <2 hours. Overall, the median positive cluster ion (0.8-2 nm) concentrations was higher
508 than that of negative cluster ions, as can be expected from the Earth's electrode effect (Hoppel,
509 W. A., 1967). However, during the rain-events 0.8-2 nm and 2-4 nm negative ions dominated
510 over similar-size positive ions. Similar, but weaker, rain-events were found at the site outside
511 the rainforest canopy (T3).

512 Outside the rainforest canopy, we observed a clear diel pattern in the cluster ion concentration
513 during both wet and dry season, with higher concentrations during the morning and evening
514 compared with other times of the day. The results from the PSM showed a very similar pattern:
515 the median diel cycle of >1.5 nm particles showed a higher concentration in the early morning
516 and a dip in the afternoon followed by an increase in the evening after sunset. The diel pattern
517 was less pronounced inside the canopy, which indicates that the rainforest canopy acts as a sink
518 for newly formed particles and hinders vertical mixing.

519 We observed eight NPF events showing particle growth at site T3 outside the canopy during
520 Jan-Oct 2014, which is the wet season. The formation rates were considerably higher for
521 neutral particles compared with ions during the NPF events. The growth rates of newly formed
522 ions and particles were comparable to each other and showed a clear increase with increasing
523 size in the sub-20 nm size range. We found two different regimes for the 3-7 nm size range.
524 We found 3 out of 8 NPF days with GR of about 2 nm h⁻¹ and 4 out of 8 NPF days with GR of
525 about 14 nm h⁻¹. The sulfuric acid concentrations were the same for the nucleation event days
526 and non-event days (approx. 9*10⁵ cm⁻³). The back trajectory calculations using HYSPLIT did
527 not show any clear difference between days with small GR compared to days with high GR.
528 Nevertheless, a clear difference in air mass origin on NPF days compared to the same number
529 of days without NPF was observed. Most likely the observed growth on all the NPF days is
530 driven by highly oxidized organic compounds (Tröstl et al., 2016). The back trajectory
531 calculations show air mass origin over rainforest area on NPF days, vs the Amazon river on days
532 where no NPF was observed. As shown by the SMPS, the particles grew to sizes of around 60
533 nm during all the NPF events, which means they are able to act as cloud condensation nuclei
534 (McFiggans et al, 2006; Andreae and Rosenfeld, 2008; Kerminen et al. 2012). There were clear
535 differences in median cluster and intermediate ion concentrations between the NPF event days
536 and non-event days for the time window of 09:00-12:00 LT. The median cluster ion
537 concentration was lower, and the median intermediate ion concentration was higher by a factor
538 of 1.6, during the NPF event days compared with non-event days. The condensation sink was



539 lower during the NPF event days (0.0016) compared with non-event days (0.005). No
540 precipitation was observed on any of the NPF event days. Most likely, during the dry season
541 the condensation sink is too high for new particle formation.

542

543 **Acknowledgements**

544 We acknowledge the Academy of Finland Centre of Excellence program (grant no. 272041).
545 We acknowledge the Atmospheric Radiation Measurement (ARM) Climate Research Facility,
546 a user facility of the United States Department of Energy, Office of Science, sponsored by the
547 Office of Biological and Environmental Research, and support from the Atmospheric System
548 Research (ASR) program of that office. D.W. wishes to acknowledge the Austrian Science
549 Fund (FWF, grant no J-3951). P Artaxo acknowledges FAPESP project 2013/05014-0 and
550 CNPq for funding. We thank field support from Alcides Ribeiro, Bruno Takeshi and Fabio
551 Jorge. We acknowledge logistical support from the LBA Central Office, at the INPA – Instituto
552 Nacional de Pesquisas da Amazonia.

553

554 **References**

- 555 Aalto, P., Hameri, K., Becker, E., Weber, R., Salm, J., Makela, J. M., Hoell, C., O'Dowd, C.
556 D., Karlsson, H., Hansson, H. C., Vakeva, M., Koponen, I. K., Buzorius, G. and Kulmala, M.,
557 Physical characterization of aerosol particles during nucleation events, *Tellus series B –*
558 *Chemical and physical meteorology*, 53:4, 344-358; DOI: 10.1034/j.1600-0889.2001.530403.x
559
- 560 Andreae, M. O.: Aerosols before pollution, *Science*, 315, 50–51, 2007.
- 561 Andreae, M. O. and Rosenfeld D.: Aerosol-cloud-precipitation interactions. Part 1. The nature
562 and sources of cloud-active aerosols, *Earth-Science Reviews*; 89, 13-41, 2008,
563 DOI: 10.1016/j.earscirev.2008.03.001
564
- 565 Andreae, M. O., Acevedo, O. C., Araújo, A., Artaxo, P., Barbosa, C. G. G., Barbosa, H. M. J.,
566 Brito, J., Carbone, S., Chi, X., Cintra, B. B. L., da Silva, N. F., Dias, N. L., Dias- Júnior, C. Q.,
567 Ditas, F., Ditz, R., Godoi, A. F. L., Godoi, R. H. M., Heimann, M., Hoffmann, T., Kesselmeier,
568 J., Könemann, T., Krüger, M. L., Lavric, J. V., Manzi, A. O., Lopes, A. P., Martins, D. L.,
569 Mikhailov, E. F., Moran-Zuloaga, D., Nelson, B. W., Nölscher, A. C., Santos Nogueira, D.,
570 Piedade, M. T. F., Pöhlker, C., Pöschl, U., Quesada, C. A., Rizzo, L. V., Ro, C.-U.,
571 Ruckteschler, N., Sá, L. D. A., de Oliveira Sá, M., Sales, C. B., dos Santos, R. M. N., Saturno,
572 J., Schöngart, J., Sörgel, M., de Souza, C. M., de Souza, R. A. F., Su, H., Targhetta, N., Tóta,
573 J., Trebs, I., Trumbore, S., van Eijck, A., Walter, D., Wang, Z., Weber, B., Williams, J.,



- 574 Winderlich, J., Wittmann, F., Wolff, S., and Yáñez-Serrano, A. M.: The Amazon Tall Tower
575 Observatory (ATTO): overview of pilot measurements on ecosystem ecology, meteorology,
576 trace gases, and aerosols, *Atmos. Chem. Phys.*, 15, 10723–10776, doi:10.5194/acp-15-
577 10723-2015, 2015.
- 578 Artaxo, P., Rizzo, L. V., Brito, J. F., Barbosa, H. M. J., Arana, A., Sena, E. T., Cirino, G. G.,
579 Bastos, W., Martin, S. T., and Andreae, M. O.: Atmospheric aerosols in Amazonia and land
580 use change: from natural biogenic to biomass burning conditions, *Faraday Discuss.*, 165, 203–
581 235, 2013.
- 582 Asmi, E., Sipilä, M., Manninen, H. E., Vanhanen, J., Lehtipalo, K., Gagné, S., Neitola, K.,
583 Mirme, A., Mirme, S., Tamm, E., Uin, J., Komsaare, K., Attoui, M., and Kulmala, M.: Results
584 of the first air ion spectrometer calibration and intercomparison workshop, *Atmos. Chem. Phys.*,
585 9, 141-154, doi:10.5194/acp-9-141-2009, 2009.
- 586 Backman, J., Rizzo, L. V., Hakala, J., Nieminen, T., Manninen, H. E., Morais, F., Aalto, P. P.,
587 Siivola, E., Carbone, S., Hillamo, R., Artaxo, P., Virkkula, A., Petäjä, T., and Kulmala, M.: On
588 the diurnal cycle of urban aerosols, black carbon and the occurrence of new particle formation
589 events in springtime São Paulo, Brazil, *Atmos. Chem. Phys.*, 12, 11733-11751,
590 doi:10.5194/acp-12-11733-2012, 2012.
- 591
- 592 Dunne E., Gordon H., Kürten A., Almeida J., Duplissy J., Williamson C., Ortega I. K.,
593 Pringle J.K., Adamov A., Baltensperger U., Barmet P., Benduhn F., Bianchi F.,
594 Breitenlechner M., Clarke A., Curtius J., Dommen J., Donahue N. M., Ehrhart S., Flagan R.
595 C., Franchin A., Guida R., Hakala J., Hansel A., Heinritzi M., Jokinen T., Kangasluoma J.,
596 Kirkby J., Kulmala M., Kupc A., Lawler M. J., Lehtipalo K., Makhmutov V., Mann G.,
597 Mathot S., Merikanto J., Miettinen P., Nenes A., Onnela A., Rap A., Reddington C. L. S.,
598 Riccobono F., Richards N. D. A., Rissanen M. P., Rondo L., Sarnela N., Schobesberger S.,
599 Sengupta K., Simon M., Sipilä M., Smith J. N., Stozkhov Y., Tomé A., Tröstl, J., Wagner P.
600 E., Wimmer D., Winkler P. M., Worsnop D. R., Carslaw K. S., Global atmospheric particle
601 formation from CERN CLOUD measurements, *Science*, 354: 6316, 2016.
- 602
- 603 Dos Santos, V. N., Herrmann, E., Manninen, H. E., Hussein, T., Hakala, J., Nieminen, T.,
604 Aalto, P. P., Merkel, M., Wiedensohler, A., Kulmala, M., Petaja, T. and Hameri, K., *Atmos.*
605 *Chem. Phys.*, 15; 23:13717-13737, DOI: 10.5194/acp-15-13717-2015, 2015.
- 606 Hakkinen, S. A. K., Manninen, H. E., Yli-Juuti, T., Merikanto, J., Kajos, M. K., Nieminen, T.,
607 D'Andrea, S. D., Asmi, A., Pierce, J. R., Kulmala, M. and Riipinen, I.: Semi-empirical
608 parameterization of size-dependent atmospheric nanoparticle growth in continental
609 environments, *Atmos. Chem. Phys.*, 13, 15: 7665-7682, doi: 10.5194/acp-13-7665-2013, 2013.
- 610
- 611 Harrison, R. G. and Carslaw K. S., Ion-Aerosol-cloud processes in the lower atmosphere,
612 *Reviews of Geophysics*, 41, 3 / 1012, doi:10.1029/2002RG000114, 2003.
- 613



- 614 Hirsikko, A., Laakso, L., Horrak, U., Aalto, P. P., Kerminen, V.-M. and Kulmala, M., Annual
615 and size dependent variation of growth rates and ion concentrations in boreal forest, *Bor*
616 *Environ Res*, 10, 357-369, 2005.
- 617 Hirsikko, A., Bergman, T., Laakso, L., Dal Maso, M., Riipinen, I., Horrak, U. and Kulmala,
618 M., Identification and classification of the formation of intermediate ions measured in boreal
619 forest, *Atmos. Chem. Phys.*, 7, 201-210, 2007.
- 620 Hirsikko, A., Nieminen, T., Gagne, S., Lehtipalo, K., Manninen, H. E., Ehn, M., Horrak, U.
621 Kerminen, V.-M., Laakso, L., McMurry, P. H., Mirme, A., Mirme, S., Petaja, T., Tammet, H.,
622 Vakkari, V., Vana, M., Kulmala, M. Atmospheric ions and nucleation: a review of
623 observations, *Atmos. Chem. Phys.*, 11, 767-798, DOI: 10.5194/acp-11-767-2011, 2011.
- 624 Hoppel, W. A., Theory of the electrode effect, *Journal of Atmospheric and Terrestrial Physics*,
625 Vol. 22, 1967.
- 626 Horrak, U, Salm, J and Tammet, H, Bursts of intermediate ions in atmospheric air, *JOURNAL*
627 *OF GEOPHYSICAL RESEARCH-ATMOSPHERES*, 103: 13909-13915, DOI:
628 10.1029/97JD01570, 1998.
- 629
630 Hörrak, U., Tammet, H., Aalto, P. P., Vana, M., Hirsikko, A.,
631 Laakso, L., and Kulmala, M.: Formation of charged particles
632 associated with rainfall: atmospheric measurements and lab experiments,
633 *Rep. Ser. Aerosol Sci.*, 80, 180–185, 2006.
- 634
635 Kalivitis, N., Stavroulas, I., Bougiatioti, A., Kouvarakis, G., Gagné, S., Manninen, H. E.,
636 Kulmala, M., and Mihalopoulos, N.: Night-time enhanced atmospheric ion concentrations in
637 the marine boundary layer, *Atmos. Chem. Phys.*, 12, 3627-3638, doi:10.5194/acp-12-3627-
638 2012, 2012.
- 639
640 Kangasluoma J., Kuang C., Wimmer D., Rissanen M. P., Lehtipalo K., Ehn M., Worsnop, D.
641 R., Wang, J., Kulmala M. and Petäjä T., Sub-3nm particle size and composition dependent
642 response of a nano-CPC battery, *Atmos. Meas. Tech.*, 7, 689–700, doi:10.5194/amt-7-689-
643 2014, 2014.
- 644
645 Kerminen, V.-M, Paramonov, M., Anttila, T., Riipinen, I., Fountoukis, C, Korhonen, H., Asmi,
646 E., Laakso, L., Lihavainen, H., Swietlicki, E., Svenningsson, B., Asmi, A., Pandis, S. N,
647 Kulmala, M. and Petaja, T., Cloud condensation nuclei production associated with atmospheric
648 nucleation: a synthesis based on existing literature and new results, *Atmos. Chem. Phys.*, 12,
649 24: 12037-12059; doi: 10.5194/acp-12-12037-2012, 2012.
- 650
651 Kontkanen J., Lehtipalo K., Ahonen L., Kangasluoma J., Manninen H. E., Hakala J., Rose C.,
652 Sellegri K., Xiao S., Wang L., Qi X., Nie W., Ding A., Yu H., Lee S., Kerminen V.-M.,



- 653 Petäjä T. And Kulmala M., Measurements of sub-3 nm particles using a particle size
654 magnifier in different environments: from clean mountain top to polluted megacities
655 *Atmos. Chem. Phys.*, 2163–2187; doi:10.5194/acp-17-2163-2017, 2017.
656
- 657 Kulmala, M., Vehkamäki, H., Petaja, T., Dal Maso, M., Lauri, A., Kerminen, VM, Birmili,
658 McMurry, PH. Formation and growth rates of ultrafine atmospheric particles: a review of
659 observations, *J. Aerosol Sci.*, 35,143-176, 2004.
660
- 661 Kulmala, M., Petäjä, T., Nieminen, T., Sipilä, M., Manninen, H. E., Lehtipalo, K., Dal Maso,
662 M., Aalto, P. P., Junninen, H., Paasonen, P., Riipinen, I., Lehtinen, K. E. J., Laaksonen, A., and
663 Kerminen, V.-M.: Measurement of the nucleation of atmospheric aerosol particles, *Nat.*
664 *Protoc.*, 7, 1651–1667, 2012.
665
- 666 Kulmala, M., Kontkanen, J., Junninen, H., Lehtipalo, K., Manninen, HE, Nieminen, T.,
667 Petaja, T., Sipila, M., Schobesberger, S., Rantala, P., Franchin, A., Jokinen, T., Jarvinen, E.,
668 Aijala, M., Kangasluoma, J., Hakala, J., Aalto, P. P., Paasonen, P., Mikkila, J., Vanhanen, J.,
669 Aalto, J., Hakola, H., Makkonen, U., Ruuskanen, T., Mauldin, R. L., III, Duplissy, J.,
670 Vehkamäki, H., Back, J., Kortelainen, A., Riipinen, I., Kurten, T., Johnston, M. V., Smith, J.
671 N. Ehn, M., Mentel, T. F., Lehtinen, K. E. J., Laaksonen, A., Kerminen, V.-M. Worsnop, D.
672 R., Direct Observations of Atmospheric Aerosol Nucleation, *Science*, 339, 943, 2013.
673
- 674 Kulmala, M., Petaja, T. Ehn, M., Thornton, J., Sipila, M., Worsnop, D. R., Kerminen, V. -M.,
675 Chemistry of Atmospheric Nucleation: On the Recent Advances on Precursor
676 Characterization and Atmospheric Cluster Composition in Connection with Atmospheric
677 New Particle Formation, *Annu. Rev. Phys. Chem.*, 65, 21–37, 2014.
678
- 679 Kulmala, M., Luoma, K., Virkkula, A, Petaja, T., Paasonen, P., Kerminen, V.-M. Nie, W.,
680 Qi, X., Shen, Y., Chi, X., Ding, A., On the mode-segregated aerosol particle number
681 concentration load: contributions of primary and secondary particles in Hyytiälä and Nanjing
682 *Boreal Environment Research*, 21, 319-331, 2016.
683
- 684 Leino, K., Nieminen, T., Manninen, H. E., Petaja, T., Kerminen, V.-M. and Kulmala, M.,
685 Intermediate ions as a strong indicator of new particle formation bursts in a boreal forest,
686 *BOREAL ENVIRONMENT RESEARCH*, 21, 274-286, 2016.
687
- 688 Lelieveld J., Butler, T. M., Crowley, J. N., Dillon, T. J., Fischer, H., Ganzeveld, L., Harder,
689 H., Lawrence, M. G., Martinez, M., Taraborrelli, D., Williams, J., Atmospheric oxidation
690 capacity sustained by a tropical forest, *Nature* 452, 737-740, 2008.
691
- 692 Manninen, H. E., Nieminen, T., Asmi, E., Gagné, S., Häkkinen, S., Lehtipalo, K., Aalto, P.,
693 Vana, M., Mirme, A., Mirme, S., Hörrak, U., Plass-Dülmer, C., Stange, G., Kiss, G., Hoffer,
694 A., Törö, N., Moerman, M., Henzing, B., de Leeuw, G., Brinkenberg, M., Kouvarakis, G. N.,
695 Bougiatioti, A., Mihalopoulos, N., O'Dowd, C., Ceburnis, D., Arneth, A., Svenningsson, B.,



- 696 Swietlicki, E., Tarozzi, L., Decesari, S., Facchini, M. C., Birmili, W., Sonntag, A.,
697 Wiedensohler, A., Boulon, J., Sellegri, K., Laj, P., Gysel, M., Bukowiecki, N., Weingartner,
698 E., Wehrle, G., Laaksonen, A., Hamed, A., Joutsensaari, J., Petäjä, T., Kerminen, V.-M., and
699 Kulmala, M.: EUCAARI ion spectrometer measurements at 12 European sites – analysis of
700 new particle formation events, *Atmos. Chem. Phys.*, 10, 7907-7927, doi:10.5194/acp-10-7907-
701 2010, 2010.
- 702
- 703 Manninen, H. E., Mirme, S., Mirme, A., Petäjä, T., and Kulmala, M.: How to reliably detect
704 molecular clusters and nucleation mode particles with Neutral cluster and Air Ion Spectrometer
705 (NAIS), *Atmos. Meas. Tech.*, 9, 3577-3605, doi:10.5194/amt-9-3577-2016, 2016.
- 706
- 707 Martin, S. T., Andreae, M. O., Artaxo, P., Baumgardner, D., Chen, Q., Goldstein, A. H.,
708 Guenther, A., Heald, C. L., Mayol-Bracero, O. L., McMurry, P. H., Pauliquevis, T., Poeschl,
709 U., Prather, K. A., Roberts, G. C., Saleska, S. R., Silva Dias, M. A., Spracklen, D. V.,
710 Swietlicki, E., Trebs, I., SOURCES AND PROPERTIES OF AMAZONIAN AEROSOL
711 PARTICLES, REVIEWS OF GEOPHYSICS, 48, RG2002, DOI: 10.1029/2008RG000280,
712 2010a.
- 713
- 714 Martin, S. T., Andreae, M. O., Althausen, D., Artaxo, P., Baars, H., Borrmann, S., Chen, Q.,
715 Farmer, D. K., Guenther, A., Gunther, S. S., Jimenez, J. L., Karl, T., Longo, K., Manzi, A.,
716 Müller, T., Pauliquevis, T., Petters, M. D., Prenni, A. J., Pöschl, U., Rizzo, L. V., Schneider,
717 J., Smith, J. N., Swietlicki, E., Tota, J., Wang, J., Wiedensohler, A., and Zorn, S. R.: An
718 overview of the Amazonian Aerosol Characterization Experiment 2008 (AMAZE-08), *Atmos.*
719 *Chem. Phys.*, 10, 11415–11438, doi:10.5194/acp-10-11415-2010, 2010b.
- 720
- 721 Martin, S. T., Artaxo, P., Machado, L. A. T., Manzi, A. O., Souza, R. A. F., Schumacher, C.,
722 Wang, J., Andreae, M. O., Barbosa, H. M. J., Fan, J., Fisch, G., Goldstein, A. H., Guenther, A.,
723 Jimenez, J. L., Pöschl, U., Silva Dias, M. A., Smith, J. N., and Wendisch, M.: Introduction:
724 Observations and Modeling of the Green Ocean Amazon (GoAmazon2014/5), *Atmos. Chem.*
725 *Phys.*, 16, 4785-4797, doi:10.5194/acp-16-4785-2016, 2016.
- 726
- 727
- 728 S. T. Martin, P. Artaxo, L. Machado, A. O. Manzi, R. A. F. Souza, C. Schumacher, J. Wang,
729 T. Biscaro, J. Brito, A. Calheiros, K. Jardine, A. Medeiros, B. Portela, S. S. de Sá, K. Adachi,
730 A. C. Aiken, R. Albrecht, L. Alexander, M. O. Andreae, H. M. J. Barbosa, P. Buseck, D. Chand,
731 J. M. Comstock, D. A. Day, M. Dubey, J. Fan, J. Fast, G. Fisch, E. Fortner, S. Giangrande, M.
732 Gilles, A. H. Goldstein, A. Guenther, J. Hubbe, M. Jensen, J. L. Jimenez, F. N. Keutsch, S.
733 Kim, C. Kuang, A. Laskin, K. McKinney, F. Mei, M. Miller, R. Nascimento, T. Pauliquevis,
734 M. Pekour, J. Peres, T. Petäjä, C. Pöhlker, U. Pöschl, L. Rizzo, B. Schmid, J. E. Shilling, M.
735 A. Silva Dias, J. N. Smith, J. M. Tomlinson, J. Tóta, and M. Wendisch, The Green Ocean
736 Amazon Experiment (GoAmazon2014/5) observes pollution affecting gases, aerosols, clouds



- 737 and rainfall over the rain forest, *Bull. Am. Meteor. Soc.*, DOI:10.1175/BAMS-D-15-00221.1,
738 2017.
- 739
- 740 Mather, J. H. and Voyles, J. W.: The ARM Climate Research Facility: A review of structure
741 and capabilities, *Bull. Am. Meteor. Soc.*, 94, 377–392, 2013.
- 742 McFiggans, G, Artaxo, P., Baltensperger, U., Coe, H., Facchini, M. C., Feingold, G., Fuzzi, S.,
743 Gysel, M., Laaksonen, A., Lohmann, U., Mentel, T. F., Murphy, D. M., O'Dowd, C. D., Snider,
744 J. R.) and Weingartner, E., The effect of physical and chemical aerosol properties on warm
745 cloud droplet activation, *Atmos. Chem. Phys.*, 6, 2593-2649, 2006.
- 746 Merikanto, J., Spracklen, D. V., Mann, G. W., Pickering, S. J., and Carslaw, K. S.: Impact of
747 nucleation on global CCN, *Atmos. Chem. Phys.*, 9, 8601-8616, doi:10.5194/acp-9-8601-2009,
748 2009.
- 749 Nieminen, T., Yli-Juuti, T., Manninen, H. E., Petäjä, T., Kerminen, V.-M., and Kulmala, M.:
750 Technical note: New particle formation event forecasts during PEGASOS–Zeppelin Northern
751 mission 2013 in Hyytiälä, Finland, *Atmos. Chem. Phys.*, 15, 12385-12396, doi:10.5194/acp-
752 15-12385-2015, 2015.
- 753 Nieminen, T., Lehtinen, K. E. J. and Kulmala, M., Sub-10 nm particle growth by vapor
754 condensation - effects of vapor molecule size and particle thermal speed, *Atmos. Chem. Phys.*,
755 10, 9773-9779; DOI: 10.5194/acp-10-9773-2010, 2010.
- 756 Rose, C., Sellegri, K., Velarde, F., Moreno, I., Ramonet, M., Weinhold, K., Krejci, R. Ginot,
757 P., Andrade, M., Wiedensohler, A. and Laj, P., Frequent nucleation events at the high altitude
758 station of Chacaltaya (5240 m a.s.l.), Bolivia, *ATMOSPHERIC ENVIRONMENT*, 102, 18-
759 29, DOI: 10.1016/j.atmosenv.2014.11.015, 2015.
- 760 Tammet, H., Hörrak, U., and Kulmala, M.: Negatively charged nanoparticles produced by
761 splashing of water, *Atmos. Chem. Phys.*, 9, 357-367, doi:10.5194/acp-9-357-2009, 2009.
- 762 Tröstl, J., Chuang, W. K., Gordon, H., Heinritzi M., Yan C., Molteni U., Ahlm L., Frege C.,
763 Bianchi F., Wagner R., Simon M., Lehtipalo K., Williamson C., Craven J. S., Duplissy J.,
764 Adamov A., Almeida J., Bernhammer A.-K., Breitenlechner M., Brilke S., Dias A., Ehrhart S.,
765 Flagan R. C., Franchin A., Fuchs C., Guida R., Gysel M., Hansel A., Hoyle C. R., Jokinen T.,
766 Junninen H., Kangasluoma J., Keskinen H., Kim J., Krapf M., Kürten A., Laaksonen A.,
767 Lawler M., Leiminger M., Mathot S., Möhler O., Nieminen T., Onnela A., Petäjä T., Piel F. –
768 M., Miettinen P., Rissanen M. P., Rondo L., Sarnela N., Schobesberger S., Sengupta K., Sipilä
769 M., Smith J. N., Steiner G., Tomè A., Virtanen A., Wagner A.C., Weingartner E., Wimmer D.,
770 Winkler P. M., Ye P., Carslaw K. S., Curtius J., Dommen J., Kirkby J., Kulmala M., Riipinen
771 I., Worsnop D.R., Donahue N. M. and Baltensperger U., The role of low-volatility organic
772 compounds in initial particle growth in the atmosphere, *Nature*, 533, 527-531,
773 doi:10.1038/nature18271, 2016.



774

775 Vanhanen, J., Mikkilä, J., Lehtipalo, K., Sipilä, M., Manninen, H. E., Siivola, E., Petäjä, T.,
776 and Kulmala, M.: Particle size magnifier for nano-CN detection. *Aerosol Sci. Technol.*,
777 45:533–542, 2011.

778

779 Suni, T., Kulmala, M., Hirsikko, A., Bergman, T., Laakso, L., Aalto, P. P., Leuning, R., Cleugh,
780 H., Zegelin, S., Hughes, D., van Gorsel, E., Kitchen, M., Vana, M., Hörrak, U., Mirme, S.,
781 Mirme, A., Sevanto, S., Twining, J., and Tardos, C.: Formation and characteristics of ions and
782 charged aerosol particles in a native Australian Eucalypt forest, *Atmos. Chem. Phys.*, 8, 129-
783 139, doi:10.5194/acp-8-129-2008, 2008.

784

785 Svenningsson, B., Arneth, A., Hayward, S., Holst, T., Massling,
786 A., Swietlicki, E., Hirsikko, A., Junninen, H., Riipinen, I., Vana,
787 M., Dal Maso, M., Hussein, T., and Kulmala, M.: Aerosol particle
788 formation events and analysis of high growth rates observed
789 above a subarctic wetland-forest mosaic, *Tellus*, 60B, 353–364,
790 2008

791

792 Vana M., Kulmala, M., Dal Maso M. and Hörrak, U., Comparative study of nucleation mode
793 aerosol particles and intermediate air ions formation events at three sites, *Journal of*
794 *Geophysical Research*, VOL. 109, D17201, doi:10.1029/2003JD004413, 2004

795

796

797 Vana, M., Ehn, M., Petaja, T., Vuollekoski, H., Aalto, P., de Leeuw, G., Ceburnis, D., O'Dowd,
798 C. D. and Kulmala, M. Characteristic features of air ions at Mace Head on the west coast of
799 Ireland,
800 *ATMOSPHERIC RESEARCH*, 90, 278-286, DOI: 10.1016/j.atmosres.2008.04.007, 2008.

801

802 Vanhanen, J., Mikkilä, J., Lehtipalo, K., Sipilä, M., Manninen, H. E., Siivola, E., Petäjä, T. and
803 Kulmala, M. (2011), Particle Size Magnifier for Nano-CN Detection, *Aerosol Science and*
804 *Technology*, 45: 4, 533 — 542, DOI: 10.1080/02786826.2010.547889, 2011.

805

806 Wagner, R., Manninen, H. E., Franchin, A., Lehtipalo, K., Mirme, S., Steiner, G., Petäjä, T.
807 and Kulmala, M.: On the accuracy of ion measurements using a Neutral cluster and Air Ion
808 Spectrometer, *Boreal Environment Research*, 21, 230-241, 2016.

809 Wang J., Krejci R., Giangrande S., Kuang, C., Barbosa H. M. J., Brito J., Carbone S., Chi X.,
810 Comstock J., Ditas F., Lavric J., Manninen H. E., Mei F., Moran-Zuloaga D., Pöhlker C.,
811 Pöhlker M. L., Saturno J., Schmid B., Souza R. A. F., Springston S. R., Tomlinson J. M., Toto
812 T., Walter D., Wimmer D., Smith J. N., Kulmala M., Machado L.A. T., Artaxo P., Andreae M.
813 O., Petäjä T. & Martin S. T., Amazon boundary layer aerosol concentration sustained by
814 vertical transport during rainfall, *Nature*, doi:10.1038/nature19819, 2016.

815



816 Wang, M. and Penner, J. E.' Aerosol indirect forcing in a global model with particle nucleation,
817 *Atmos. Chem. Phys.*, 9:1, 239-260, 2009.

818

819 Yu, F. and Luo, G.' Simulation of particle size distribution with a global aerosol model:
820 contribution of nucleation to aerosol and CCN number concentrations, *Atmos. Chem. Phys.*, 9:
821 20, 7691-7710, 2009.

822

823

824

825

826

827

828

829

830

831

832

833

834

835

836

837

838

839

840

841

842

843 **Tables**

844 Table 1. A comparison between the sites during wet and dry season. Outside canopy site values
845 on the left, inside canopy on the right. The months chosen for the wet season for inside the
846 canopy are Jan-Mar and Dec-Mar for inside the canopy. Dry season includes Aug-Oct and
847 July-Sept for outside and inside canopy. Aerosol and ion parameters from the NAIS
848 measurements listed are ion concentrations in three size bins (0.8-2, 2-4 and 4-20 nm). Neutral
849 particle concentrations in two different size bins from the NAIS (2-4 and 4-20 nm) and total
850 particle concentrations (>10 nm) from CPC measurements and condensation sink from the
851 SMPS. The numbers present diel medians and in brackets 25th-75th percentiles. Environmental
852 parameters are temperature, relative humidity, precipitation, wind direction.



854

	Outside canopy (T3)		Inside canopy (T0t)	
Particle and ion concentrations				
	<i>Wet</i>	<i>Dry</i>	<i>Wet</i>	<i>Dry</i>
Cluster ions (0.8-2 nm) [cm⁻³]	1000 (-) (836-1500)	988 (-) (688-1400)	814 (-) (641-1051) 968(+) (790-1178)	605(-) (465-801) 765(+) (604-1003)
Intermediate ions (2-4 nm) [cm⁻³]	7 (-) (3-14)	8 (-) (4-16)	5(-) (2-10) 11(+) (7-17)	4(-) (2-8) 11(+) (7-16)
Large ions (4-20 nm) [cm⁻³]	58 (-) (27-107)	56 (-) (30-106)	84(-) (40-178) 147(+) (62-410)	132(-) (52-425) 162 (80-329)
Intermediate particles (2-4 nm) [cm⁻³]	579 (286-943)	550 (276-927)	477 (252-810)	591 (323-1003)
Large particles (4-20 nm) [cm⁻³]	1000 (547-2150)	922 (552-1600)	308 (169-690)	530(-) (250-1070)
CPC total particles (>10 nm) [cm⁻³]	1000 (533-1352)	731 (411-2000)	-	-
SMPS condensation sink [s⁻¹]	1.5 e-3	5 e-3	-	-
Environmental parameters				
Temp [°C]	25.7	26.1	24 (23-25)	24 (23-26)
RH [%]	94.8	92.8	97 (93-98)	96 (90-98)
Precipitation [mm hr⁻¹]	49	32	0.7186	0.4248
Wind direction [°; relative to north]	92.6	112.7	97 (58-143)	97 (60-147)

855

856

857



859 Table 2. Annual statistics for ion and total particle concentration in T0t inside canopy site for
860 the period of 2011-2014. Values represent median (25th-75th percentiles).

861

Size bin	Negative ion	Positive ions	Total particles
0.8-2 nm	723 (537-1012)	879 (683-1124)	-
2-4 nm	5 (2-9)	10 (7-16)	521 (278-889)
4-20 nm	85 (40-182)	151 (68-382)	380 (192-872)

862

863 Table 3. New particle formation (NPF) characteristics at the outside canopy (T3) site.
864 Classified NPF event and rain-induced ion event frequencies.

865

	NPF days	Undefined	Non-events	Rain events	No-rain events
Wet season (Jan-Mar)	8/65 (12%)	0/65 (0%)	57/65 (88%)	61/65 (94%)	04/65 (6%)
Dry season (Aug-Oct)	0/49 (0%)	0/49 (0%)	49/49 (100%)	15/49 (31%)	34/49 (69%)

866

867



868 Table 4. The parameters shown are from the outside canopy site for nucleation/no nucleation
 869 event days. Median total particle concentration measured by a CPC, measured by the NAIS in
 870 two size ranges (2-4 and 4-20 nm) and negative ion concentrations from the NAIS in three size
 871 ranges (0.8-2, 2-4 and 4-20). The median values are calculated for the time window 09:00 –
 872 12:00 as this is the time window of NPF events. The numbers in the brackets represent the 25th
 873 and 75th percentile. The second part of the table includes median numbers of environmental
 874 parameters for the whole day: temperature, RH, Precipitation and wind direction for NPF /no
 875 NPF days. The main differences are the condensation sink and the wind direction.
 876

Particle and ion concentrations		
09:00 – 12:00 LT		
	NPF day	Non NPF day
Cluster ions (0.8-2 nm) [cm ⁻³]	800 (-) (692-905)	870 (-) (687-1000)
Intermediate ions (2-4 nm) [cm ⁻³]	13 (-) (6-23)	8 (-) (4-15)
Large ions (4-20 nm) [cm ⁻³]	83 (-) (44-137)	62 (-) (25-119)
Intermediate particles (2-4 nm) [cm ⁻³]	606 (303-969)	547 (522-1600)
Large particles (4-20 nm) [cm ⁻³]	1000 (604-1600)	970 (238-1000)
Full day data		
SMPS Condensation sink [s ⁻¹]	1e-3	5e-3
CPC total particles (>10 nm) [cm ⁻³]	1100 (579-1860)	1000 (404-2000)
Environmental parameters		
full day		
	NPF day	Non NPF day
Temp [°C]	26.5	25.9
RH [%]	90.6	93.6
Precipitation [mm hr⁻¹]	0	0.002
Wind direction [°; relative to north]	81.6	105.8

877

878



879 Table 5. Growth rates (GR, nm h^{-1}) and nucleation rates (J; $\text{cm}^{-3}\text{s}^{-1}$) determined from the NAIS
 880 ion and particle data for each nucleation event. Also the median values for the condensation
 881 sink (CS; s^{-1}) for each event day are shown. The GR were determined by finding the maximum
 882 concentration for different size bins for 2-3 nm, 3-7nm and 7-20 nm. The GR values present
 883 median values of the GR for positive and negative ions. The nucleation rates represent median
 884 numbers for positive and negative ions. The GR between ions and particles agree well with
 885 each other for the individual nucleation events. GR are smaller for the smaller size ranges and
 886 increase with particle size. The nucleation rates are in general higher for the particles than the
 887 ions. The Condensation is calculated from the SMPS size distributions.
 888

Size bins	2-3 nm				3-7 nm						
	Particles		ions		Particles		Ions		Particles		
	GR (nm h^{-1})	J ($\text{cm}^{-3}\text{s}^{-1}$)	GR (nm h^{-1})	J ($\text{cm}^{-3}\text{s}^{-1}$)	GR (nm h^{-1})	J ($\text{cm}^{-3}\text{s}^{-1}$)	GR (nm h^{-1})	J ($\text{cm}^{-3}\text{s}^{-1}$)	GR (nm h^{-1})	J ($\text{cm}^{-3}\text{s}^{-1}$)	CS (s^{-1})
29.01.2014	0.8	0.19	1.4	0.003	2.8	0.097	1.7	0.001	-	-	-
30.01.2014	-	-	3.7	0.011	13.6	-	7.1	0.13	4.4	0.38	0.0007
06.02.2014	0.8	-	19.8	0.07	29	0.87	11	0.01	24	0.28	0.0016
12.02.2014	0.7	0.17	1.2	0.005	1.3	0.09	1.2	0.003	3	0.09	0.0016
12.03.2014	1.1	0.2	1.7	0.002	13.3	-	11.2	0.008	4.9	-	0.0014
13.03.2014	1.5	0.2	1.6	-	1.2	-	8	-	13.6	0.24	0.0015
18.03.2014	-	-	0.7	0.002	-	-	7.7	0.009	-	-	0.0017
25.03.2014	0.8	0.11	-	-	15.7	0.4	15.8	0.018	14	0.18	0.0017



Figures

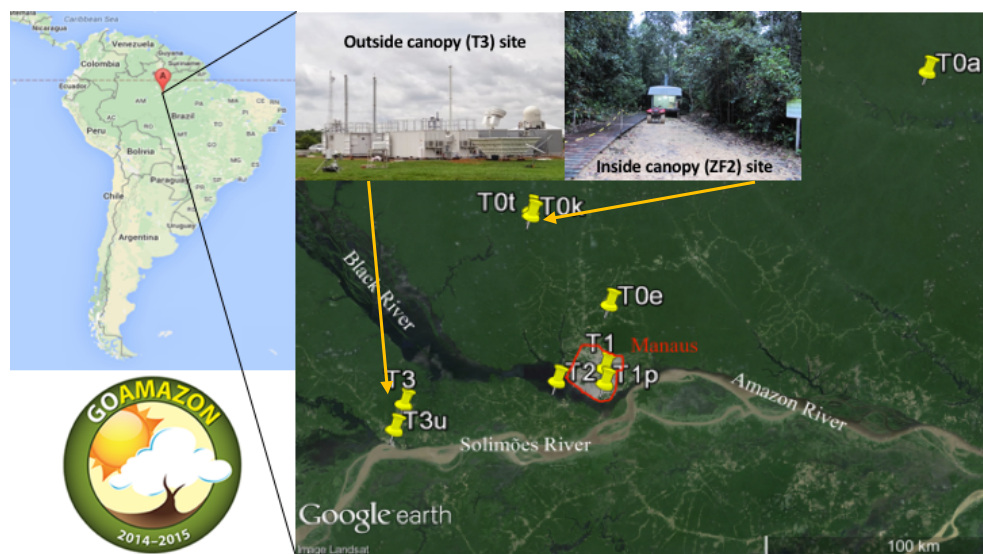


Figure 1. Location on map and photos of the inside canopy (T0t) and outside canopy (T3) sampling sites in Amazonas. The left column shows a map of South America and the right side shows a satellite view and photos of the T0t and T3 environment. From the inside canopy site we present the long term data, whereas from the outside canopy site we show the comparison of wet and dry season. The inside canopy measurements at T0t is located in a pristine area, whereas the outside canopy site is located at T3, downwind of Manaus.

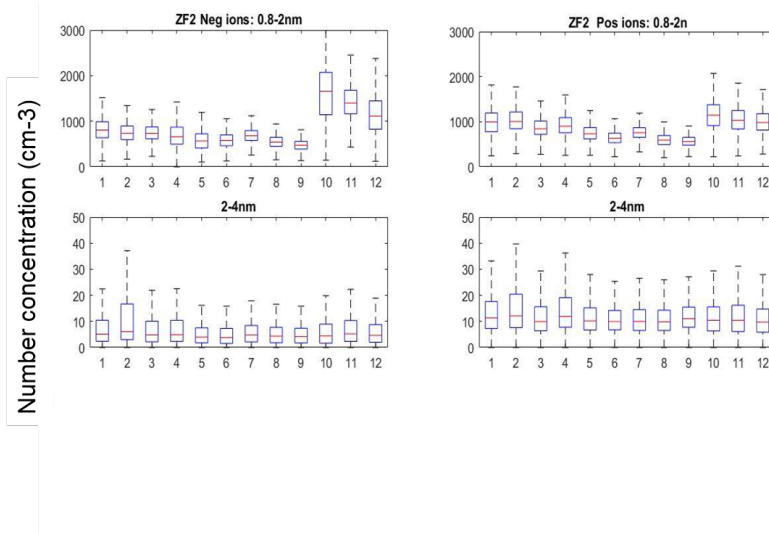


Figure 2. Annual variation of the negative (left column) and positive (right column) ion concentrations for 2011–2014 from inside the rainforest canopy. The bars represent median monthly ion concentrations, and the whiskers represent 25th and 75th percentiles.

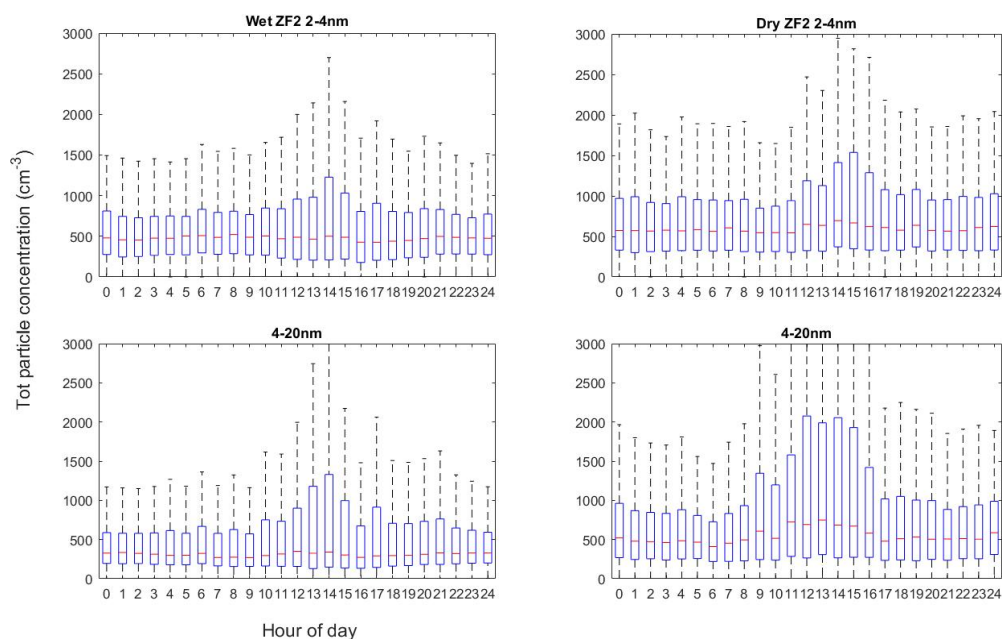




Figure 3. Diel cycle of total particle concentration at the inside canopy site (T0t) during the wet (Dec-Mar; left) and dry (Apr-Oct; right) season, for 2-4 nm (top) and 4-20 nm (bottom) particles.

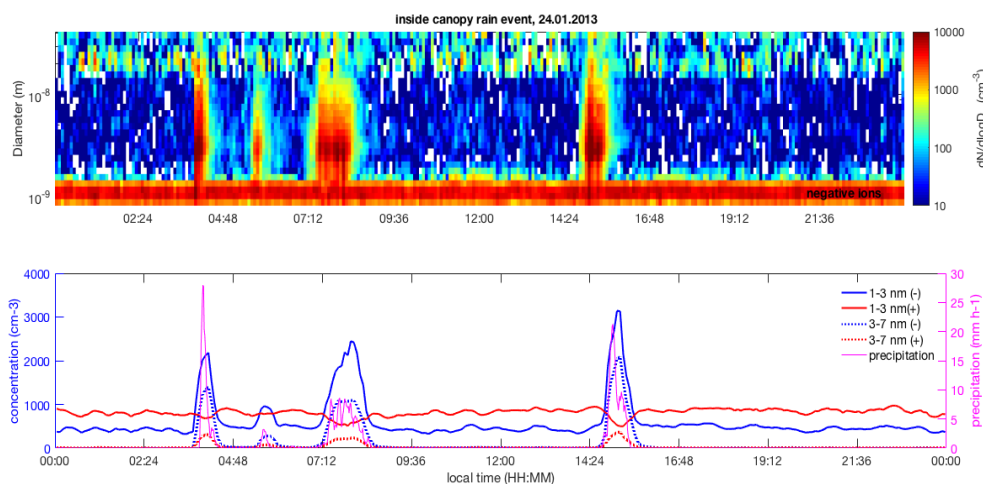


Figure 4. Typical rain-induced event at the inside canopy (T0t) site (Jan 24, 2013). Upper panel: negative ion number size distribution during a selected rain-induced ion production day measured with the NAIS. Lower panel: precipitation in mm h^{-1} (pink trace) on the right axis, concentration of small (1-3 nm) negative (blue) and positive (red) ions with the scale on the left axis.

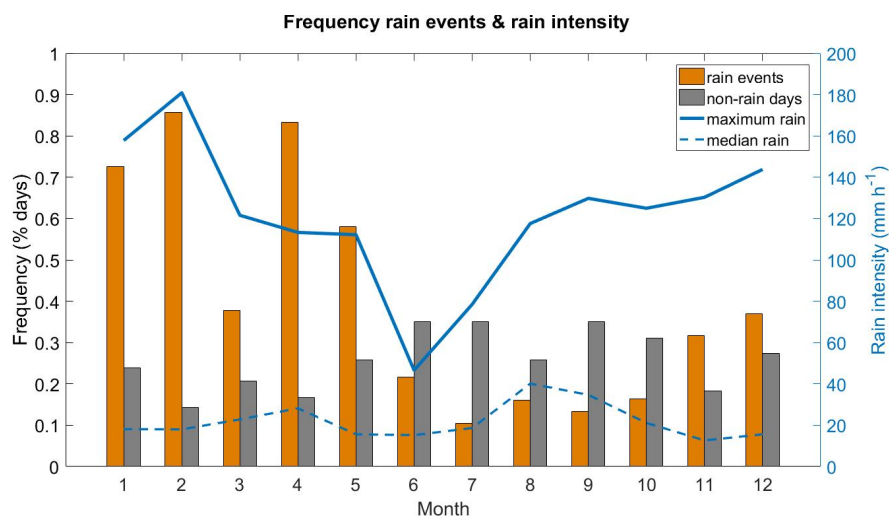


Figure 5. Inside canopy site (T0t) monthly frequencies (% of days with available data) of rain-induced ion events ($n=306$) and no-rain days ($n=195$). Dashed line indicates the median monthly variation of rain intensity (mm h^{-1}). Data collected continuously from September 2011 to January 2014 at the T0t site.

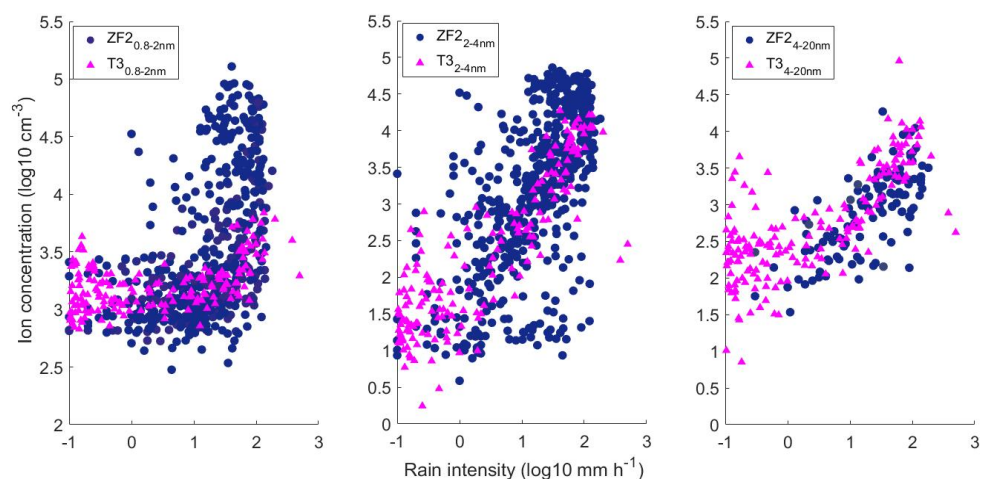


Figure 6. Median daily ion concentrations as a function of rain intensity at the inside canopy site (T0t) between September 2011 and January 2014 (blue circles). Outside canopy site (T3) rain events concentrations are added for comparison (triangles). (A) Cluster ions (0.8-2 nm), (B) 2-4 nm, and (C) 4-20 nm.

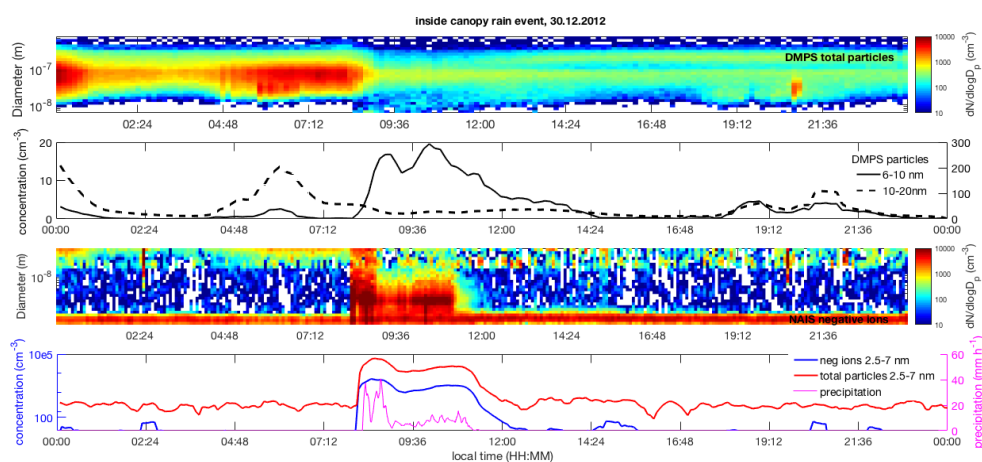


Figure 7. Example for a rain-induced event for total particles (DMPS). The DMPS measurements are taken above the canopy (60 m height), NAIS measurements are inside the canopy. Panel (a) shows the DMPS surface Figure. Panel (b) shows the particles measured by the DMPS for 6-10 nm and 10-20 nm (dashed line). (c) shows the surface Figure for the negative ions, measured by the NAIS. (d) shows the negative ion concentrations for 2.5-7 nm in blue and the total particle concentration in the same size range from the NAIS in red with the scale on the left axis. The pink trace shows the precipitation in mm h^{-1} on the right axis.

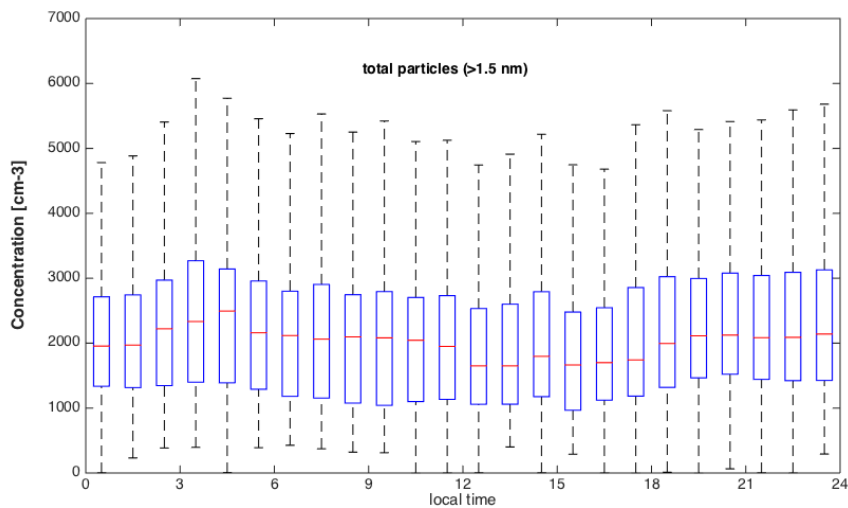


Fig 8. Diel cycle of particles bigger than 1.5 nm measured by the PSM during the dry season outside the rainforest canopy. In total, 38 days of data were used. The data shows hourly median concentrations, the whiskers 25th and 75th percentile.

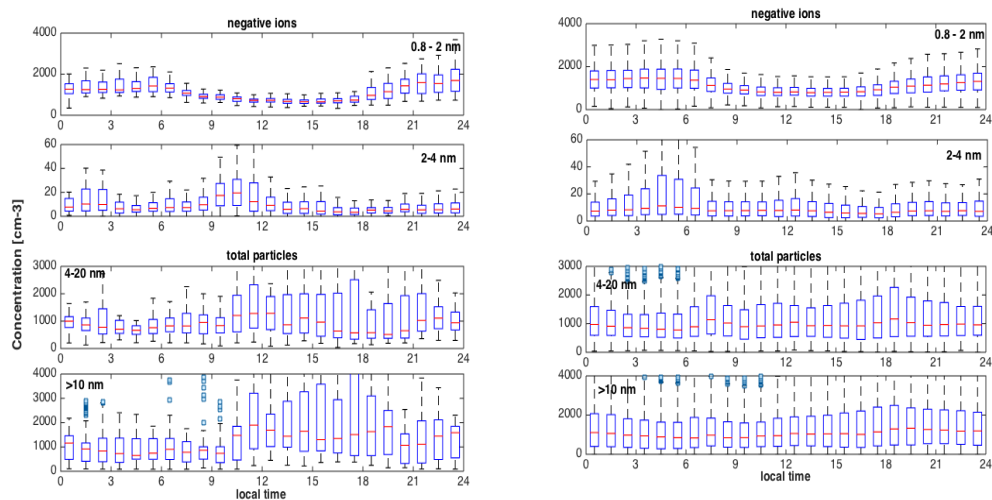


Figure 9. Diel cycle of aerosol particles and ions measured outside the canopy by the NAIS (small: 0.8–2 nm; intermediate: 2–4 nm; large: 4–20 nm) and total particles >10 nm as measured by the MAOS CPC. The left column shows the NPF event days and the right column the non NPF days. The markers are hourly median number concentrations and the whiskers 25th and 75th percentiles.

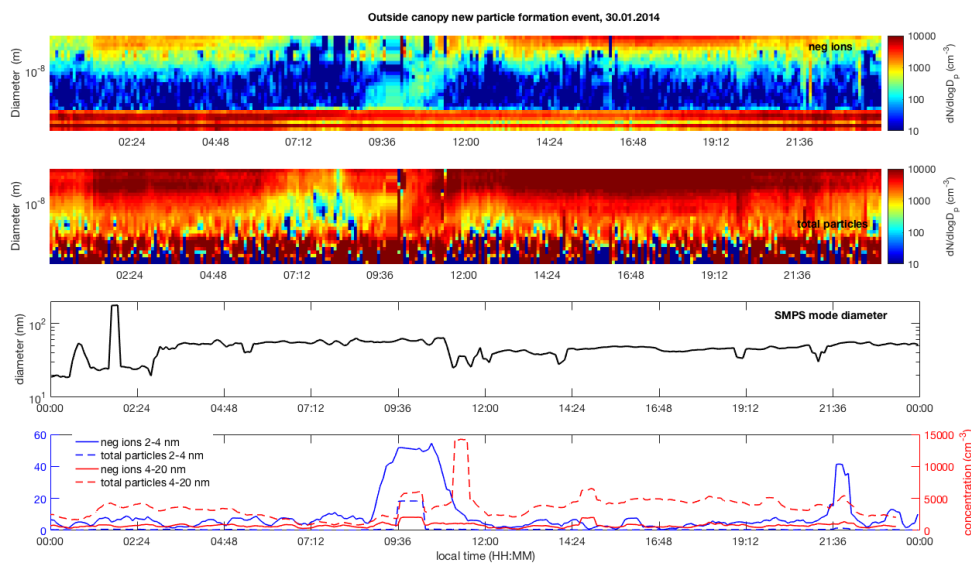


Figure 10. One example NPF day as observed at the outside canopy (T3) site. (a) and (b) show the surface Figures from the NAIS, (a) for negative ions, (b) for total particles. The color code indicates the measured concentrations. Panel (c) shows the mode diameter as measured by the MAOS SMPS. The mode diameter decreases at the start of the NPF event followed by continuous growth up to about 60 nm. Panel (d) shows negative ion and neutral particle concentrations in two size ranges (2-4 nm and 4-20 nm). Note the left axis is for the 2-4 nm ion concentration and 2-4 nm particle concentrations, right 4-20 neutral particle and ion concentrations.